
Structure and refractive properties of LiNaSO₄ single crystals

^{1,2} Shchepanskyi P. A., ³ Kushnir O. S., ¹ Stadnyk V. Yo., ¹ Brezvin R. S. and ⁴ Fedorchuk A. O.

¹ Physics Faculty, Ivan Franko National University of Lviv, 19 Dragomanov Street, 79005 Lviv, Ukraine, pavloshchepanskyi@gmail.com

² Institute of Physics, J. Dlugosh University in Czestochowa, Armii Krajowej 13/15, PL-42-201, Czestochowa, Poland

³ Faculty of Electronics and Computer Technologies, Ivan Franko National University of Lviv, 107 Tarnavsky Street, 79017 Lviv, Ukraine

⁴ Department of Inorganic and Organic Chemistry, Lviv National University of Veterinary Medicine and Biotechnologies, 50 Pekarska Street, 79010 Lviv, Ukraine

Received: 14.04.2018

Abstract. We report experimental results on the structure, refractive indices and birefringence of LiNaSO₄ (LSS) crystals. Spectral behaviours of the refractive indices and the birefringence of LSS at the room temperature, as well as temperature and baric dependences of the birefringence are discussed. We examine the refractive indices and the birefringence using Lorentz–Lorenz and simplified Sellmeier formulae and energy-band structure calculations. Unlike LiKSO₄, the birefringence of LSS decreases with increasing temperature, while accidental optically isotropic states are absent under the normal conditions. A significant increase in the birefringence of LSS, if compared with LiKSO₄, is assumed to be linked with asymmetry appearing in the local second-coordination environment of the LSS structure.

Keywords: lithium–sodium sulphate, ABSO₄ crystals, structure, refractive indices, birefringence, optical anisotropy.

PACS: 78.20.Ci, 78.20.Hp, 81.40.Vw

UDC: 535.323, 535.5, 535.012, 548.0

1. Introduction

Dielectric crystals of ABSO₄ family attract a permanent attention of researchers stipulated by their ferroelectric, ferroelastic and superionic properties. This also concerns a subgroup LiBSO₄, with A = Li and B = Li, Na, K, NH₄, Rb, It is known that one of its representatives, lithium–sodium sulphate LiNaSO₄ (or LSS), reveals two phases, a low-temperature β-phase and a high-temperature α-phase, with a structural transition occurring at ~ 788 K [1]. The α-modification of LSS has a multisectoral cubic structure and manifests fast ionic conductivity, while the room-temperature β-LSS phase is characterized by trigonal symmetry and belongs to the spatial group *P31c* [2].

In general, there is rich data on different physical properties of LSS crystals. In particular, much attention has been given to their structure [1–4], electrical [5, 6], thermal [1, 7] and luminescent [8, 9] properties. Nuclear magnetic resonance [10, 11], as well as infrared and Raman spectra [12, 13], have also been studied. Moreover, pyroelectric properties of LSS have been revealed [4]. Some of the recent works have also indicated practical possibilities for using LSS in solid-state fuel cells [14] and dosimetry [15].

Curiously enough, the optical characteristics of the β-LSS crystals are known in much less detail. The exception is the fundamental-absorption edge and the corresponding dispersion [16].

It is known that, most likely, the transitions corresponding to the photon energies near the fundamental edge of LSS are indirect allowed, with the direct bandgap and the effective phonon energy being equal respectively to $E_g = 4.7$ eV and $E_p = 0.6$ eV. On the other hand, such basic optical characteristics as refractive indices and birefringence, which represents a measure of optical anisotropy in LSS, are also of great importance. As far as we know, there is no data concerned with these characteristics, except for the refractive indices for a single wavelength (~ 589.3 nm) and a mention that LSS is optically uniaxial [4]. Among different aspects, an interest to the optical anisotropy is due to the fact that the ABSO_4 -group crystals often reveal inversion of sign of the optical birefringence, or simply 'isotropic point' [17–20]. The latter is interesting from the fundamental point of view [21, 22] and, moreover, finds its applications in a number of practical fields [23–25]. Since the isotropic point has been observed in structurally close LiKSO_4 crystals [17], it would be interesting to consider the effect of cation substitution on the optical anisotropy and examine the presence of the phenomenon in LiNaSO_4 .

The aim of the present work is to study the structure of the LSS crystals and their refractive and birefringent properties. A supplementary task is comparing the structure and the optical anisotropy of LSS with those of the other representatives of ABSO_4 family and, first of all, with the characteristics of optically uniaxial LiKSO_4 crystals.

2. Experimental

Single crystals of LSS were grown from aqueous solution, using a slow-evaporation method (see, e.g., the work [20] and references therein). The starting compounds were commercially available Li_2SO_4 and Na_2SO_4 salts with the purity of 99.9%. The crystals thus obtained had the shape of triangular prisms with the volume ~ 0.7 cm³. They showed excellent optical quality.

The studies of crystal structure were performed on powders using a standard X-ray technique, of which peculiarities are described in the work [20]. Spectral dependences of the refractive indices $n_i(\lambda)$ and the optical birefringence $\Delta n_i(\lambda)$ were measured along the principal axes $i = x, y$ and z of the optical Fresnel ellipsoid (see Ref. [20]). The curves $n_i(\lambda)$ were studied at the room temperature (294 K), and $\Delta n_i(\lambda)$ at $T = 294, 430, 565$ and 635 K. The $\Delta n_i(T)$ dependence was obtained using a standard polarization-interference technique. The tolerance of the temperature control was not less than ± 0.1 K.

To study the effect of uniaxial mechanical stresses on the birefringence, we employed a special cryostat attachment that allowed for compressing crystal samples at fixed temperatures. The maximal pressures used in our experiments were equal to $\sigma_i = 200$ bar.

3. Structural characteristics

Experimental and theoretical diffractograms are shown in Fig. 1. The structure of the LSS crystals has been refined using a Rietveld method and WinCSD software [26], issuing from the space group $P31c$ ($Z = 6$). Some of the structural information is displayed in Table 1. We have obtained the cell parameters $a = 7.6299(2)$ Å and $c = 9.8597(2)$ Å. The standard structural-difference factors are equal to $R_1 = 0.0424$, $R_p = 0.0674$, $R_{wp} = 0.0924$ and $R_{exp} = 0.0461$, whereas the goodness of fit amounts to $\text{GoF} = 2.0$. Our results agree fairly well with the lattice parameters $a = 7.6270$ Å and $c = 9.8579$ Å reported in Ref. [2].

The crystalline structure of the LSS crystals represents an assembly of anionic tetrahedra $(\text{SO}_4)^{2-}$ and cation atoms (see Fig. 2). To study the structure of LSS in a more detail, the approach of second-coordination environment has been used (see Ref. [27] for further explanations).

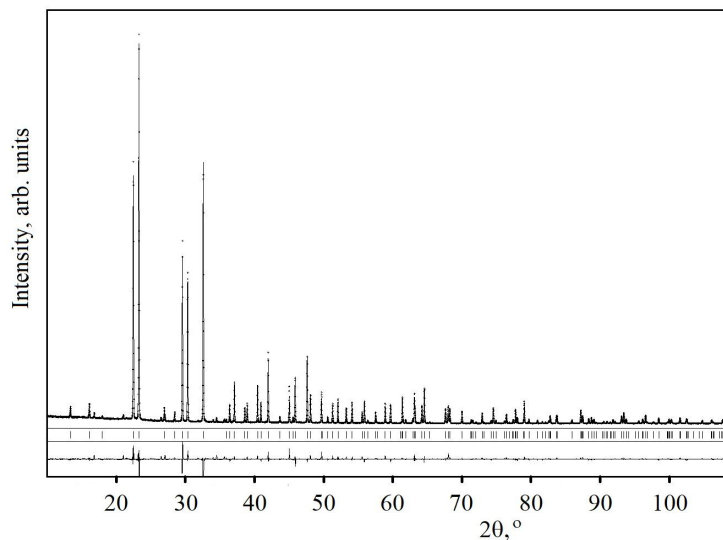


Fig. 1. Experimental (data points), theoretical (upper solid line) and differential (lower solid line) diffractograms obtained for LSS. Vertical bars correspond to the Bragg-reflection marks determined for refined LSS structure.

Panels (a), (b) and (c) in Fig. 3 illustrate the second-coordination environments of the anions that are formed around three different sulphur atoms (the notations S1, S2 and S3) in the structure of LSS. For the anions associated with the atoms S1 and S2, the second-coordination environments represent imperfect hexagonal analogues of cuboctahedra, while for the anions corresponding to the S3 atoms we have a deformed hexagonal prism, with additional anions located against the base faces. Li and Na atoms occupy respectively tetrahedral and octahedral cavities within the environment.

Table 1. Wyckoff positions, fractional atomic coordinates x/a , y/b and z/c , and isotropic thermal-displacement factor B obtained for our LSS crystals at 294 K. The lattice cell volume is equal to $497.09(5) \text{ \AA}^3$. The figures in parentheses represent standard deviations.

Atom	Wyckoff position	x/a	y/b	z/c	$B, \text{ \AA}^2$
Li	$6c$	0.0250(1)	0.2490(1)	0.3860(9)	2.50(2)
Na	$6c$	0.0242(2)	0.5486(2)	0.1659(5)	1.22(4)
S1	$2b$	1/3	2/3	0.4591(5)	0.69(4)
S2	$2b$	1/3	2/3	0.8915(5)	0.41(4)
S3	$2a$	0	0	0.1490(4)	0.53(3)
O1	$6c$	0.1170(5)	0.2189(3)	0.2045(4)	0.58
O2	$6c$	0.4591(4)	0.2255(5)	0.0163(4)	0.58
O3	$6c$	0.4774(4)	0.1622(4)	0.3405(5)	0.58

Similarly to the other ABSO_4 -group crystals, LiKSO_4 and $\text{K}_{1.75}(\text{NH}_4)_{0.25}\text{SO}_4$ [20], the structural units in LSS are tightly arranged, which is a feature of ionic type of bonding. The other feature of domination of ionic bonds is a high-symmetry character of the second-coordination environments of anions in the shape of hexagonal analogue of cuboctahedron (see Fig. 3). When compared with the second-coordination environment of $(\text{SO}_4)^{2-}$ anions in LiKSO_4 (see Fig. 3d), one can notice a more pronounced covalent component in the bonding of LSS. It is associated with ‘imperfections’ available in the second-anion coordination of LSS, which imply a lower symmetry of local environment of the anions. Moreover, all the sulphur atoms in LiKSO_4 are structurally equivalent and have the same coordination environment, unlike the case of LSS. Another very

important feature of the second-anion environment in LiKSO_4 lies in ordering of the $(\text{SO}_4)^{2-}$ tetrahedra, which is absent in LSS. We anticipate that these structural differences and, in particular, lower local symmetry and stronger structural anisotropy of LSS, as against LiKSO_4 , have to manifest themselves in the optical properties.

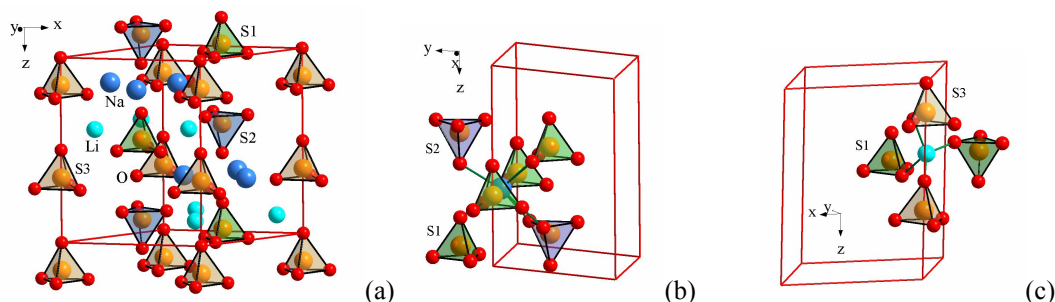


Fig. 2. General arrangement of structural fragments (a) and environments of Na^+ (b) and Li^+ (c) ions in the structure of LSS crystals. S1, S2 and S3 are structurally different sulphur atoms. Red lines frame the unit cell.

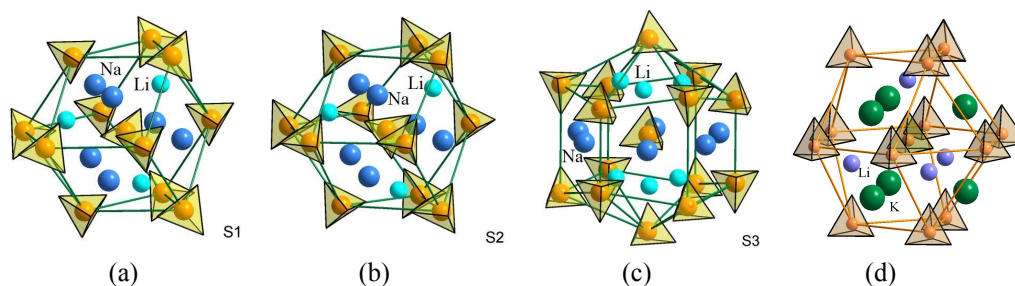


Fig. 3. Second- and third- coordination environments of $(\text{SO}_4)^{2-}$ ions (yellow tetrahedra in the centres) associated with sulphur atoms of the types S1 (a), S2 (b) and S3 (c) in LSS crystals (see Table 1). Second- coordination environment of $(\text{SO}_4)^{2-}$ ion in the structure of LiKSO_4 crystals is shown in panel (d) for comparison.

The band structure, dielectric function and the optical absorption spectra of LSS in a wide spectral range will be a subject of a separate work. Here we summarize only those results which are relevant to the present topic. The calculations of the bandgap E_g^{calc} have been performed in the local-density and generalized-gradient approximations for the density functional. Our result, $E_g \approx 5.5$ eV, is somewhat larger than the experimental value 4.7 eV. The difference of the bandgaps calculated for the $x(y)$ and z axes, which gives the bandgap anisotropy, is equal to 0.50 eV. It is comparable to the corresponding parameter obtained for $\text{K}_{1.75}(\text{NH}_4)_{0.25}\text{SO}_4$ (~ 0.53 eV [20]) and less than the result for LiKSO_4 (1.21 eV – see Ref. [28]). Almost all of the energy levels, except for the lowest ones in the conduction band near the centre of the Brillouin zone, are characterized by a weak dispersion, which is typical for the ABSO_4 group. Finally, since the long-wavelength absorption bands in LSS lie in the far infrared range, the effective infrared oscillators hardly affect the spectral behaviour of its refractive properties in the visible region.

4. Refractive indices and optical birefringence

Dispersion of the refractive indices for the LSS crystals is shown in Fig. 4a. The relations $n_x = n_y \neq n_z$ and $n_z > n_{x,y}$ hold true for the refractive indices in the entire spectral region under study. This confirms the fact that LSS is uniaxial and optically positive [4]. To describe quantitatively the refractive properties of LSS in the visible optical range, we use the two-oscillator Sellmeier relation and the Lorentz–Lorenz formula (see, e.g., explanations in Ref. [20]):

$$n_i^2 - 1 \approx \frac{B_i \lambda_{0,i}^2 \lambda^2}{\lambda_{0,i}^2 - \lambda^2} - B'_i \lambda^2, \quad (1)$$

$$\frac{n_i^2 - 1}{n_i^2 + 2} = \frac{4}{3} \pi N_0 \alpha_i = \frac{\rho}{\mu} R_i. \quad (2)$$

Here B_i and B'_i are the parameters of respectively ultraviolet and infrared effective oscillators, $\lambda_{0,i}$ denotes the position of the corresponding ultraviolet effective absorption band (the parameter $\lambda_{0,IR,i}$ of ultraviolet absorption band in Eq. (1) vanishes since $\lambda_{0,IR,i}^2 \gg \lambda^2$ – see Section 3), ρ the density of crystal (2.527 g/cm³ for LSS [2]), μ its molar mass, N_0 the atomic number density, whereas α_i and R_i imply respectively the electronic polarizability and the molar refractivity.

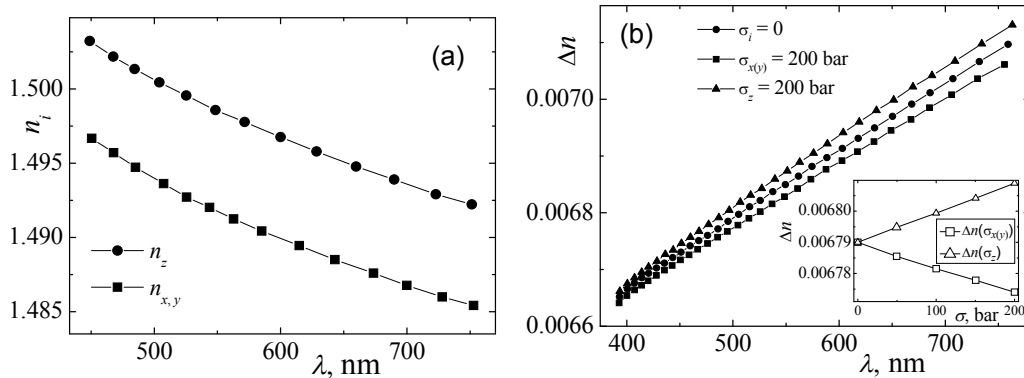


Fig. 4. Spectral dependences of refractive indices $n_i(\lambda)$ (a) and birefringence dispersions $\Delta n(\lambda)$ obtained under different uniaxial stresses (b) for the LSS crystals. Insert in panel (b) shows baric dependences of birefringence $\Delta n(\sigma)$ for different stress directions, as measured at the light wavelength $\lambda = 500$ nm. All the dependences refer to the room temperature ($T = 294$ K).

The spectral variations of the ordinary and extraordinary refractive indices are almost the same, being equal to -5.5×10^{-5} and -2.5×10^{-5} for 450 and 750 nm, respectively. The results of fitting the curves $n_i(\lambda)$ by Eqs. (1) and (2) are listed in Table 2. Basing on a commonly used additivity assumption for the partial molar refractivities of the constitutive ions, one can derive

$$R_{Li^+} + R_{Na^+} + R_{SO_4^{2-}} \approx (0.2 + 0.7 + 14.5) \text{ cm}^3/\text{mol} = 15.4 \text{ cm}^3/\text{mol}.$$

This value is only 5% larger than the experimental refractivity obtained at 500 nm and averaged over light polarizations (see Table 2). A comparison of the refractive parameters of LSS with those peculiar to LiKSO₄ [17, 28] shows that the cationic substitution $K \rightarrow Na$ leads to a slight decrease in the electronic polarizability ($\sim 7\%$) and molar refractivity ($\sim 13\%$), a displacement of the ultraviolet-oscillator position towards shorter wavelengths (~ 26 nm), and an increase of the B parameter associated with the oscillator strength ($\sim 10\%$ and $\sim 25\%$ for the x and z axes). Notice also that the refractivity parameters R for LiRbSO₄ and, especially, α -LiNH₄SO₄

Table 2. Parameters of refractive dispersion for LSS crystals at 294 K.

Principal axis i	$\lambda_{0,i}$, nm	B_i , 10^{-6} nm ⁻²	B'_i , 10^{-9} nm ⁻²	α_i , 10^{-24} cm ³ (at $\lambda = 500$ nm)	R_i , cm ³ /mol (at $\lambda = 500$ nm)
x, y	68.93	102.50	10.37	5.756	14.512
z	63.60	122.50	12.41	5.821	14.688

are essentially ($\sim 50\%$) larger than that of LSS (see Refs. [18, 19]). Nonetheless, the cationic substitution $K \rightarrow Na$ leads to nearly twice as large increase in the refractive indices, if compared with the substitutions $K \rightarrow Rb$ and $K \rightarrow NH_4$ (see discussions in Refs. [17–19]).

Fig. 4b displays spectral dependences of the birefringence measured for the LSS crystals at the room temperature. Here the central curve refers to mechanically unloaded sample, while the upper and lower ones to the samples uniaxially loaded parallel and perpendicular to the optic axis. Like in $LiKSO_4$, the dispersion $\Delta n(\lambda)$ in LSS is anomalous ($d(\Delta n)/d\lambda > 0$). It changes insignificantly in the visible range ($d(\Delta n)/d\lambda = 1.9 \times 10^{-6}$ for 400 nm, 1.2×10^{-6} for 750 nm and 1.3×10^{-6} on the average). It is worth noting that LSS reveals a rather high optical anisotropy as for the crystals of $ABSO_4$ group, with only $(NH_4)_2SO_4$ and $\beta-LiNH_4SO_4$ having still higher anisotropy.

A comparison of the birefringence values found for LSS and $LiKSO_4$ at 500 nm [17] demonstrates that the Δn parameter of LSS (0.0064) is more than order of magnitude larger than that of $LiKSO_4$ (0.0006). Perhaps, the only possible explanation of this great difference is notably different second-anion coordination environments of $LiNaSO_4$ and $LiKSO_4$ (see Section 3). At least, all the other structural characteristics of these crystals that spring to mind are close to each other. In particular, this concerns the lattice parameters and the bandgap, as well as their anisotropies (see Refs. [17, 28]). Finally, a relatively high optical anisotropy of LSS should imply the absence of optically isotropic state under the normal conditions.

As seen from Fig. 4b, the uniaxial stresses directed parallel and perpendicular to the z axis of the LSS crystals give rise to the birefringence changes, which are almost the same in the magnitude but opposite in their signs. Note that increase (or decrease) in the optical anisotropy observed under the mechanical pressure parallel (or normal) to the optic axis is also characteristic for the uniaxial $LiKSO_4$ crystals [17, 28]. The dispersion effect in the corresponding $\Delta n(\lambda)$ curve for LSS is weakened under the influence of the stress $\sigma \perp z$ and strengthened in the alternative case of $\sigma \parallel z$ (see Table 3). As seen from Fig. 4b (insert), the baric dependences of the birefringence $\Delta n(\sigma)$ are practically linear. If compared with the $(NH_4)_2SO_4$ and $RbKSO_4$ crystals, the birefringence of LSS is nearly twice as less sensitive to the mechanical stresses.

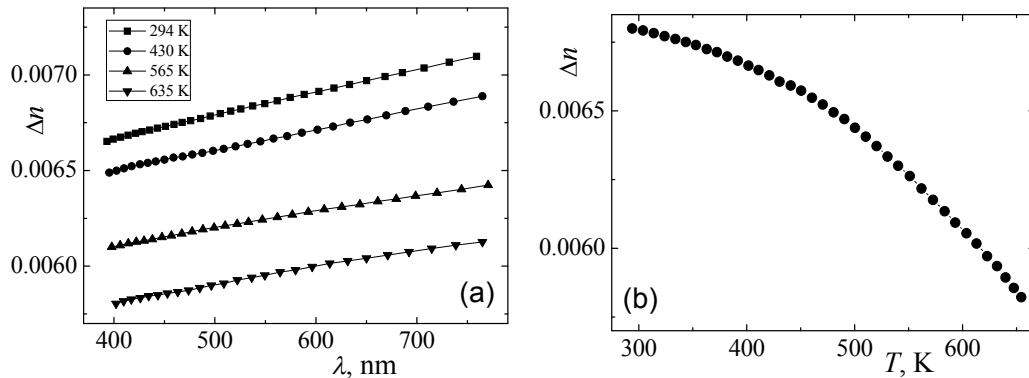
Fig. 5a illustrates the influence of temperature on the spectral dependence of the birefringence $\Delta n(\lambda)$ for the LSS crystals. As seen from the figure, the optical anisotropy decreases with increasing temperature. Averaging over the data available for different wavelengths (see Table 4) testifies that the dispersive changes in the birefringence in fact decrease with increasing temperature. As seen from Fig. 5b, the temperature dependence of the birefringence detected at fixed wavelength ($\lambda = 500$ nm) is notably nonlinear. Its quantitative characteristics are also shown in Table 4.

Table 3. Characteristics of baric changes found in the birefringence dispersion $\Delta n(\lambda)$ for the LSS crystals, as measured at $T = 294$ K.

Wavelength λ , nm	Light propagation direction	$-d(\Delta n)/d\lambda, 10^{-6} \text{ nm}^{-1} (\sigma_i = 200 \text{ bar})$			
		$\sigma = 0$	σ_x	σ_y	σ_z
400	x	1.70	–	1.56	1.72
	y		1.56	–	
550	x	1.12	–	1.11	1.27
	y		1.11	–	
750	x	1.14	–	1.02	1.16
	y		1.02	–	

Table 4. Characteristics of temperature dependence of the birefringence $\Delta n(T)$ and influence of temperature on the birefringence dispersion $\Delta n(\lambda)$ for the LSS crystals.

Temperature, K	$d(\Delta n)/dT, 10^{-5} \text{ K}^{-1}$ (at $\lambda = 500 \text{ nm}$)	$d(\Delta n)/d\lambda, 10^{-6} \text{ nm}^{-1}$		
		$\lambda = 400 \text{ nm}$	$\lambda = 550 \text{ nm}$	$\lambda = 750 \text{ nm}$
294	-0.7	1.70	1.12	1.14
430	-1.9	1.53	1.06	1.01
565	-3.9	1.13	0.87	0.81
635	-4.8	1.7	1.01	0.66

**Fig. 5.** (a) Spectral dependences of optical birefringence $\Delta n(\lambda)$ for the LSS crystals, as obtained at different temperatures: 294, 430, 565 and 635 K; (b) Temperature dependence of birefringence $\Delta n(T)$ for the LSS crystals, as obtained at the light wavelength $\lambda = 500 \text{ nm}$.

It is worthwhile that the birefringence of a close relative of LSS, the uniaxial LiKSO_4 crystal, increases with increasing temperature [28], whereas the behaviour of LSS is just the opposite. It is obvious that a decrease in the optical anisotropy of LSS observed with increasing temperature represents a general tendency associated with the fact that the LSS structure transforms gradually into its cubic version typical for the high-temperature α -phase.

6. Conclusions

In this work we present the experimental results for the structure, energy-band structure, refractive properties and optical birefringence of the LSS crystals grown from aqueous solution. We have studied their crystalline structure at the room temperature, including the main structural features refined using the approach of second-coordination environment. In general, the structure of LSS reveals dense packing of the structural units and a relatively high symmetry of the second-coordination environment, which represent characteristic features that confirm the ionic bonding. On the other hand, some evidence of a covalent component of the bonding can be seen in the LSS crystals, if compared with its closest structural analogue, LiKSO_4 . They include a violation of the above symmetry for the local anionic environment.

We have studied experimentally spectral behaviours of the refractive indices and the birefringence of LSS, as well as temperature and baric dependences of the birefringence. The dispersions of the refractive index and the birefringence in the visible range are normal and anomalous, respectively. It has been demonstrated that, unlike the situation with LiKSO_4 , the birefringence of LSS decreases with increasing temperature. Basing on the theoretical calculations of energy-band structure, we have examined the parameters of the refraction and birefringence in the frame of the Lorentz–Lorenz and simplified Sellmeier models.

The analysis has shown that the cationic substitution $K \rightarrow Na$ in the $ABSO_4$ system increases notably the refractive indices, if compared with the influence of substitutions $K \rightarrow Rb$ and $K \rightarrow NH_4$. Moreover, the $K \rightarrow Na$ replacement leads to birefringence increase by more than an order of magnitude. We assume that high optical anisotropy of the LSS crystals can be linked with asymmetry found in the second-coordination environment of their structure. Finally, we have demonstrated that there is no isotropic point in LSS under the normal conditions.

References

1. Freiheit H-Ch, Kroll H and Putnis A, 1998. The trigonal-to-cubic phase transition in $LiNaSO_4$: An X-ray and calorimetric study. *Zeit. Krist.* **213**: 575–584.
2. Morosin B and Smith D L, 1967. The crystal structure of lithium sodium sulphate. *Acta Cryst.* **22**: 906–910.
3. Pina C M and Woensdregt C F, 2001. Hartman–Perdok analysis of crystal morphology and interface topology of β - $LiNaSO_4$. *J. Cryst. Growth.* **233**: 355–366.
4. Karppinen M, 2015. Crystal structure, atomic net charges and electric moments in pyroelectric $LiNaSO_4$ at 296 K. *Acta Cryst. B.* **71**: 334–341.
5. Gundusharma U M, MacLean C and Secco E A, 1986. Rotating sulfate ion contribution to electrical conductivity in Li_2SO_4 and $LiNaSO_4$. *Solid State Commun.* **57**: 479–481.
6. Chen R H, Tseng Chaw-Ming, Shern C S and Fukami T, 2010. Ionic conductivity and dielectric relaxation studies of $LiNaSO_4$ single crystal. *Solid State Ionics.* **181**: 877–882.
7. Schroeder K, Kvist A and Ljungmark H, 1972. The phase diagrams of the binary systems Li_2SO_4 – Na_2SO_4 , Li_2SO_4 – Rb_2SO_4 , and Li_2SO_4 – Cs_2SO_4 . *Zeit. Naturforsch. A.* **27**: 1252–1256.
8. Sahare P D and Moharil S V, 1990. Thermoluminescence in $LiNaSO_4$. *Radiation Effects and Defects in Solids.* **114**: 167–172.
9. Gupta K K, Kadam R M, Dhoble N S, Lochab S P and Dhobl S J, 2018. On the study of C^{6+} ion beam and γ -ray induced effect on structural and luminescence properties of Eu doped $LiNaSO_4$: explanation of TSL mechanism by using PL, TL and EPR study. *Phys. Chem. Chem. Phys.* **20**: 1540–1559.
10. Junke K-D, Mali M, Roos J and Brinkmann D, 1988. NMR evidence for modification of the crystal structure of β - $LiNaSO_4$. *Solid State Ionics.* **28–30**: 1329–1331.
11. Shakhovoy R A, Rakhmatullin A, Deschamps M, Sarou-Kanian V and Bessada C, 2016. Nuclear magnetic resonance study of sulfate reorientations in $LiNaSO_4$. *J. Phys.: Condens. Matter.* **28**: 176003 (7 pp).
12. Teeters D and Frech R, 1982. Raman and infrared reflectivity spectra of 6LiNaSO_4 and 7LiNaSO_4 . *J. Chem. Phys.* **76**: 799–804.
13. Zhang M, Putnis A and Salje E K H, 2006. Infrared spectroscopy of superionic conductor $LiNaSO_4$: vibrational modes and thermodynamics. *Solid State Ionics.* **177**: 37–43.
14. Lv W, Tong Z, Yin Y-M, Yin J and Ma Z-F, 2015. Novel nano-composites SDC– $LiNaSO_4$ as functional layer for ITSOFC. *Nano-Micro Lett.* **7**: 268–275.
15. Puppalar S P and Dhoble S J, 2013. Development of high sensitive $LiNaSO_4$: Cu, Mg phosphor for TL dosimetry. *J. Lumin.* **137**: 245–251.
16. Abdulwahab A M, 2016. Fundamental absorption edge and normal dispersion of β - $LiNaSO_4$ single crystal. *J. Phys. Chem. Solids.* **99**: 11–18.
17. Stadnyk V I, Kushnir O S, Brezvin R S and Gaba V M, 2009. Temperature and baric changes in the refractive indices of $LiKSO_4$ crystals. *Opt. Spectrosc.* **106**: 614–620.

18. Stadnyk V Yo, Romanyuk M O and Brezvin R S, 1997. Optical and electronic parameters of RbNH_4SO_4 crystals. *Ferroelectrics*. **192**: 203–207.
19. Rudysh M Ya, Brik M G, Khyzhun O Y, Fedorchuk A O, Kityk I V, Shchepanskyi P A, Stadnyk V Yo, Lakshminarayana G, Brezvin R S, Bak Z and Piasecki M, 2017. Ionicity and birefringence of $\alpha\text{-LiNH}_4\text{SO}_4$ crystals: ab initio DFT study, X-ray spectroscopy measurements. *RSC Adv.* **7**: 6889–6901.
20. Shchepanskyi P A, Kushnir O S, Stadnyk V Yo, Fedorchuk A O, Rudysh M Ya, Brezvin R S, Demchenko P Yu and Krymus A S, 2017. Structure and optical anisotropy of $\text{K}_{1.75}(\text{NH}_4)_{0.25}\text{SO}_4$ solid solution. *Ukr. J. Phys. Opt.* **18**: 187–196.
21. Henry C H, 1966. Coupling of electromagnetic waves in CdS. *Phys. Rev.* **143**: 627–633.
22. Kushnir O and Vlokh O, 1995. Propagation of light in birefringent optically active crystals possessing linear dichroism. *Proc. SPIE.* **2648**: 585–595.
23. Yariv A and Yeh P. *Optical waves in crystals: propagation and control of laser radiation*. New York: Wiley (2003).
24. Kushnir O S, Dzendzelyuk O S, Hrabovskyy V A and Vlokh O G, 2004. Optical transmittance of dichroic crystals with ‘isotropic point’. *Ukr. J. Phys. Opt.* **5**: 1–5.
25. Bäumer Ch, Berben D, Buse K, Hesse H and Imbrock J, 2003. Determination of the composition of lithium tantalate crystals by zero-birefringence measurements. *Appl. Phys. Lett.* **82**: 2248–2250.
26. Akselrud L and Grin Y J, 2014. WinCSD: software package for crystallographic calculations (Version 4). *Appl. Cryst.* **47**: 803–805.
27. Fedorchuk A O, Parasyuk O V and Kityk I V, 2013. Second anion coordination for wurtzite and sphalerite chalcogenide derivatives as a tool for the description of anion sub-lattice. *Mater. Chem. Phys.* **139**: 92–99.
28. Stadnyk V I, Romanyuk M O, Kushnir O S, Brezvin R S, Franiv A V and Gaba V M, 2010. Temperature and spectral changes in the refractive indices of LiKSO_4 crystals under uniaxial pressures. *Int. J. Mod. Phys. B.* **24**: 6219–6233.

Shchepanskyi P. A., Kushnir O. S., Stadnyk V. Yo., Brezvin R. S. and Fedorchuk A. O. 2018. Structure and refractive properties of LiNaSO_4 single crystals. *Ukr.J.Phys.Opt.* **19**: 141 – 149. doi: 10.3116/16091833/19/3/141/2018

Анотація. У цій праці наведено експериментальні результати для структури, показників заломлення та подвійного променезаломлення (ПП) кристалів LiNaSO_4 (ЛНС). Обговорено спектральну поведінку показників заломлення та ПП кристалів ЛНС за кімнатної температури, а також температурні та баричні залежності ПП. Показники заломлення описано на підставі формули Лорентц–Лоренца, спрощеної формули Зельмеєра і розрахунків енергетичної структури. На відміну від LiKSO_4 , ПП кристалів ЛНС зменшується зі зростанням температури, а випадкові стани оптичної ізоτροпії за нормальних умов відсутні. Значне зростання ПП ЛНС, порівняно з LiKSO_4 , пов’язано з асиметрією локального другого координаційного оточення в структурі ЛНС.